Bytešníková *et al. Chem. Biol. Technol. Agric.* (2023) 10:116
https://doi.org/10.1186/s40538-023-00489-2

Chemical and Biological Technologies in Agriculture

RESEARCH

Open Access

Smart bactericide based on reduced graphene oxide decorated with copper and zinc nanoparticles

Zuzana Bytešníková[1], Jakub Pečenka[5], Dorota Tekielska[5], Jana Pekárková[1,2,3], Andrea Ridošková[1], Petr Bezdička[4], Tomáš Kiss[6], Aleš Eichmeier[5], Vojtěch Adam[1] and Lukáš Richtera[1*]

Abstract

Graphene oxide (GO) synthesised by modified Tour's method was decorated with copper and zinc nanoparticles (NPs) and simultaneously reduced by sodium borohydride to obtain a nanocomposite of reduced GO with copper and zinc NPs (rGO–Cu–Zn). The nanocomposite rGO–Cu–Zn was characterised by transmission electron microscopy (TEM), energy dispersive X-ray (EDX) spectroscopy, X-ray diffraction (XRD) and X-ray photoelectron spectroscopy (XPS). The rGO–Cu–Zn was tested against *Xanthomonas euvesicatoria* (*X. euvesicatoria*), which attacks tomatoes and causes bacterial spots (BSs), and compared with the commercial product Champion 50 WG. Total bacterial growth inhibition was observed for the 1% rGO–Cu–Zn, whereas Champion 50 WG at the same concentration inhibited but did not eradicate all the bacterial colonies. To evaluate the negative effect of the rGO–Cu–Zn on the molecular level, the expression of the genes associated with the action of abiotic and biotic stress factors was analysed. Gene expression in the plants treated with 10% rGO–Cu–Zn did not exhibit a noticeable increase.

Keywords Graphene oxide, Tomato, Bacterial spot, *Xanthomonas*, Nanoparticles

*Correspondence:
Lukáš Richtera
lukas.richtera@mendelu.cz
Full list of author information is available at the end of the article

Graphical Abstract

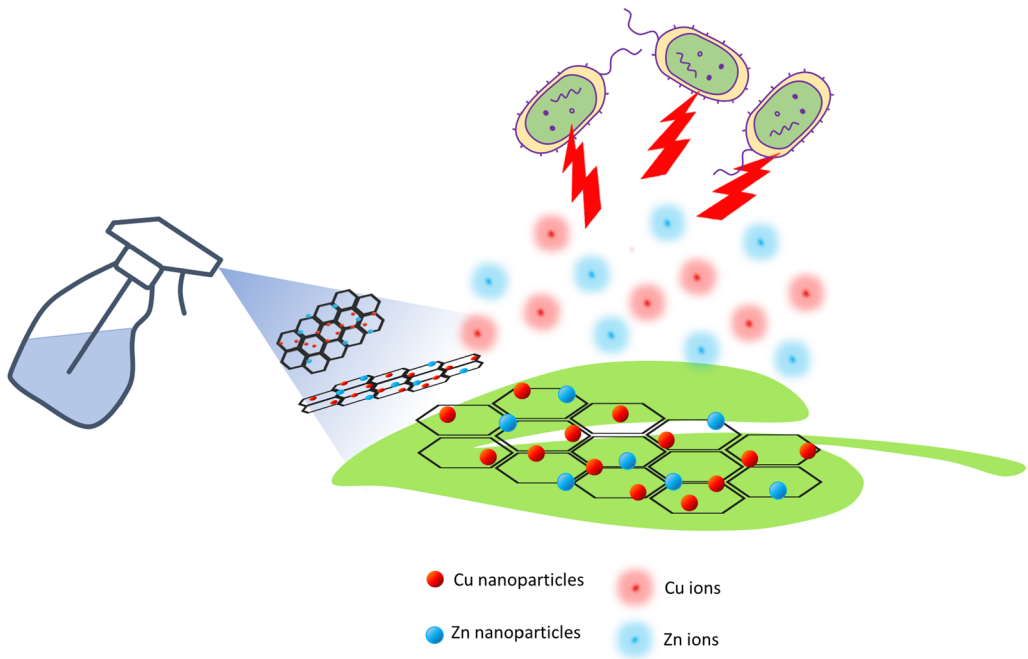

Introduction

Tomatoes are an economically important crop grown globally in fields and greenhouses. The high nutritional value of tomatoes consists of numerous bioactive compounds, such as vitamin C, provitamin A, folate, phenolic acids and flavonoids. Moreover, tomatoes are a rich source of potassium, minerals, pectin and sugars [1]. Global tomato production was over 189 million tonnes in 2021, hitting more than 16% of all vegetable crop production (1154 million tonnes in total), according to the Food and Agriculture Organization of the United Nations (FAO) report [2]. Plant bacterial diseases cause perceptible losses on a global scale annually [3–5]. BS is an important tomato and pepper disease induced by the genus *Xanthomonas*' phytopathogenic bacteria. BS of tomato caused by *X. euvesicatoria* affects all the aboveground parts of the plants [6–8]. Black necrotic spots on the shoots and leaves are followed by chlorosis and wilting, reducing the photosynthetic capacity and yield potential. Black spots on the fruit significantly reduce the crop quality and marketable yield of fresh market and processing tomatoes [9–11]. A 24–30 °C temperature range and high relative humidity create favourable conditions for spreading the disease. Serious infections of BS in the plantations can cause substantial losses, reaching 66% of the production [12–15]. Management of BS is complex and includes applying preventive measures, such as utilising disease-free seeds or seedlings, crop rotation or disease-tolerant varieties [16]. General recommendations include routine spraying of copper-based bactericides; however, effective bactericidal preparations are unavailable on the market [17].

The biocidal activity of copper has been known for centuries, and ancestors used it to cure illnesses or for sterilisation and sanitation [18]. Copper is also a trace element and an essential micronutrient in plant, animal, and human tissues. Therefore, copper is applied in agriculture not only as a protectant but also as a foliar fertiliser. The request to reduce the amount of copper needed for successful disease control is nowadays more than actual. The European Union (EU 2018/1981) regulation reduced the maximal dose allowed from 6 to 4 kg Cu/ha/year over seven years [19], a consequence of the mid-twentieth century doses as high as 50 kg Cu/ha/year being applied frequently for decades [20]. The first bactericide for crop protection used copper(II) sulphate in the *Bordeaux* mixture [21]. Nevertheless, due to high solubility in water and the penetration capacity of Cu^{2+} ions, this mixture was highly phytotoxic and, therefore, unsuitable for crop protection [22]. Other

copper-based compounds were tested and further used for crop protection against microbes, including copper(II) hydroxide or copper(II) oxide [23]. These copper-based compounds are allowed in the EU, USA and Australia. These permitted copper-based compounds are practically insoluble in water, and their Cu^{2+} ions slowly release in slightly acidic pH [24]. The limitation of these copper-based bactericides allowed in micron size is their hydrophobicity and water aggregation, decreasing their surface area and declining their antimicrobial activity [25]. NPs of these compounds offer to overcome such difficulties [26]. Several studies indicate the potential of zinc nutrition in both bulk form and as NPs to combat bacterial pathogens. The antibacterial properties of zinc oxide (ZnO) NPs were confirmed in lentils against *Pseudomonas. syringae pv. syringae* and *Xanthomonas axonopodis* pv. *phaseoli* [27] and in nutrient agar medium against *Xanthomonas campestris* pv. *beticola*, *Pseudomonas syringae* pv. *Aptata* and *Pectobacterium betavasculorum* [28]. Zinc deficiency especially appears in economically developing nations where chronic inadequate zinc intake is the main reason for malnutrition [29, 30]. There is a very close geographical relationship between human health and soil zinc deficiency, indicating an increasing need for crop biofortification using zinc [31]. Zinc can also contaminate soil, but its presence in soil has usually been related to urbanisation and industrialisation in recent years, so agriculture is not the source of zinc contamination [32]. GO and rGO are single-layer nanomaterials (depending on the definition) consisting of carbon atoms in a honeycomb lattice that primarily structurally differ in the number of present oxygen-rich function groups on their surface. NPs can decorate both nanomaterials to create functional nanocomposites to protect or supplement crops with no phytotoxicity [33, 34].

This study aims at finding the minimum amount of copper that shows the desirable effects with a minimum negative impact on the environment with nanotechnologies' assistance. Copper cannot be omitted entirely from plant protection so that the latter remains economically reasonable for farmers, but the size in the nanoscale, synergistic effect with other elements and smart carrier can create a new material that meets the requirements of all parties and brings a new concept in plant protection that aligns the green deal requirements.

Experimental section

Materials and methods

Demineralised water was produced using an Aqual 25 reverse osmosis apparatus (Aqual, Česká, Czech Republic) and further treated with Millipore System Inc. (Billerica, MA, USA) to obtain ultrapure water with a corresponding resistivity of 18.20 MΩ cm (at 25 °C). All experiments used ultrapure water unless otherwise stated. The pH values were evaluated using a pH meter (WTW inoLab, Weilheim, Germany) with a WTW SenTix pH electrode.

Synthesis of GO

The synthesis of GO was previously described in Bytešníková *et* al. [33].

Synthesis of rGO decorated concurrently with copper and zinc NPs (rGO–Cu–Zn)

The dispersion containing 50 mg of GO was diluted by 250 mL of 10 mM solution of zinc acetate dihydrate (≥ 99.0%, Sigma–Aldrich, St. Louis, MO, USA) and 250 mL solution of copper(II) acetate monohydrate (98%, VWR, Radnor, PA, USA). The mixture was stirred vigorously for 10 min at 500 rpm; then, 400 mg of sodium borohydride (98%, Sigma–Aldrich, St. Louis, MO, USA) was gradually added. The final product was three times washed with ultrapure water using a centrifuge (10 min, 6500 rcf; Universal 320, Hettich, Tuttlingen, Germany) with a total volume of 1.5 L. The final volume was 100 mL.

Synthesis of rGO decorated with copper (rGO–Cu) and zinc (rGO–Zn) NPs

The dispersion containing 50 mg of GO was diluted by 500 mL of 10 mM solution of zinc acetate dihydrate for rGO–Zn or 500 mL solution of copper acetate monohydrate for rGO–Cu. Each mixture was stirred vigorously for 10 min at 500 rpm; then, 400 mg of sodium borohydride was gradually added. The final products were trice washed with ultrapure water using a centrifuge (10 min, 6500 rcf; Universal 320, Hettich, Tuttlingen, Germany) with a total volume of 1.5 L. The final volumes were 100 mL for rGO–Cu and rGO–Zn.

Characterisation of nanomaterials

TEM with EDX spectroscopy

The sample was studied by HRTEM FEI Talos F200X and operated at 200 kV, with a maximum beam current of 1.0 nA. The lower amount of beam current was chosen not to damage the GO in the sample. The microscope was equipped with a Super-X EDX system with four silicon drift detectors, enabling element mapping. The sample was prepared on Au-grid-coated holy-carbon film.

The measured selected area electron diffraction (SAED) patterns were evaluated by ProcessDiffraction.

Scanning electron microscopy (SEM)

The morphologies of the samples were determined using SEM. The dispersed samples were diluted 1:20 with ultrapure water, applied to silicon wafers from Siegert Wafer company (Siegert Wafer GmbH, Aachen, Germany) and allowed to dry at room temperature (20–25 °C). Images of the samples were obtained using a MAIA 3 SEM (TESCAN, Brno, Czech Republic). An in-beam SE detector with an accelerating voltage of 5.0 kV, 3–4 mm working distance and 100,000–50,000-fold magnification were used. Full frame capture was performed in UH Resolution mode, and image accumulation with image shift correction was enabled; it took approximately 0.5 min with the ~0,32 µs/pixel dwell time. The spot size was set at 2.4 nm.

Correlative analysis

A correlative AFM-in-SEM analysis was performed utilising an atomic force microscope (AFM), LiteScope™ (NenoVision s.r.o., Brno, Czech Republic), inserted directly into a scanning electron microscope, MIRA3 XMU (Tescan, Brno, Czech Republic), equipped with an EDX spectroscopy detector, X-MAX 20 (Oxford Instruments PLC, Abingdon-on-Thames, UK). The analyzed area was scanned in the SEM vacuum chamber while simultaneously collecting data from AFM tip, SEM and EDX detectors. Further data post-processing were gathered using Mountains SPIP software (Digital Surf, Besançon, France).

XPS

XPS (Kratos Axis Supra with monochromatic Al K_α X-ray radiation, emission current of 15 mA and hybrid lens mode, Manchester, UK) was used to analyse the surface of the rGO–Cu–Zn nanocomposite. High-resolution spectra were measured with a pass energy of 20 eV. The spectra were fitted using a combination of Gaussian–Lorentzian line shapes in CasaXPS software 2.3.22. The Shirley algorithm was used to establish the spectra background [35].

X-ray powder diffraction (XRPD)—samples

A thin layer of a corresponding sample was deposited on a surface of a Si zero background holder (ZBH) sample by evaporating water from the suspension. All the samples prepared on ZBH were then placed into the sample holders for XRPD analysis.

XRPD – conventional Bragg–Brentano reflection geometry

Diffraction patterns were collected using a PANalytical X´Pert Pro diffractometer (Malvern PANalytical, Almelo, the Netherlands) equipped with a conventional X-ray tube (Cu K_α radiation, 40 kV, 30 mA) and a linear position sensitive detector, PIXcel, with an anti-scatter shield. A programmable divergence slit set to a fixed value of 0.25 deg., a Soller slit of 0.04 rad and a mask of 15 mm were used in the primary beam. A programmable anti-scatter slit set to a fixed value of 0.25 deg., a Soller slit of 0.04 rad and a Ni beta filter were used in the diffracted beam. Data were collected in the range of 5–90 deg. 2theta with a step of 0.0131 deg. and 500 s/step, producing a scan of about 3 h and 46 min.

Evaluation of X-ray patterns

Qualitative analysis was performed using the HighScorePlus software package, version 5.1.0 (Malvern PANalytical, Almelo, the Netherlands) [36] and the PDF-4 + database [37].

Inductively coupled plasma mass spectrometry (ICP-MS)

Samples of nanocomposites were homogenised by sonification for five minutes and further digested using a mixture of acids in the microwave digestion unit (Ultrawave, Milestone, Sorisole, Italy). Quadrupole ICP-MS Agilent 7700 × determined the total Cu, Zn and B contents. For the quality control (QC) of ICP-MS measurement, the QC sample was repeatedly analyzed—at the start and end of the measurements. Requirements for the recovery of QC samples were 80–120%.

Antibacterial activity of nanomaterials

The minimum inhibitory concentration (MIC) of the synthesized rGO–Cu–Zn was determined based on colony-forming units (CFU) enumeration. The bacterial strain *X. euvesicatoria* 2594 was purchased from the National Collection of Plant Pathogenic Bacteria. The fresh bacterial suspension ($1 \cdot 10^6$ CFU) was mixed with the rGO–Cu–Zn at the final concentrations of 1.50%, 1.00%, 0.50% and 0.25% of nanocomposite and incubated at 28 °C under continuous shaking (130 rpm) for 24 h. Then, 100 µl of treated bacterial suspension was pipetted on the centre of a sterile petri dish, and molten (45 °C) plate count agar (Himedia, India) was poured and mixed thoroughly. The positive control was prepared by replacing the tested nanocomposite with the same volume of sterile distilled water. Petri dishes were incubated at 28 °C for 40 h, and bacterial colonies were enumerated. Simultaneously, the MIC was also determined for the copper-containing commercial preparation, Champion 50 WG (Nufarm, Melbourne, Australia). The

Table 1 The list of the oligonucleotides used for the evaluation of the gene expression in tomato

Protein	Primer name	Sequence 5′ → 3′	Source
class III acidic β-1, 3-glucanase	TomQ'a-F	AAGCAAGAAGAGAGCATTAAAAGG	[39]
	TomQ'a-R	GTAATATGTTGGTTTCTTTATTAGCATATG	
class III basic β-1, 3-glucanase	PRQb-F	ACGCGTTGTTTACATCCCCTGGA	
	PRQb-R	AGTTGTTGTTGTAAGTCCTCGCGT	
glucan endo-1, 3-β-D-glucosidase	PR1-F	GGATCGGACAACGTCCTTAC	[40]
	PR1-R	GCAACATCAAAAGGGAAATAAT	
precursor of polyphenol oxidase	PoP-F	CTGATGAGGAGTACATCGCCAAG	[41]
	PoP-R	GCCACCAATTCTATAAGCACCGTTA	
catalase	CAT-F	TGGAAGCCAACTTGTGGTGT	[42]
	CAT-R	ACTGGGATCAACGGCAAGAG	
betatubulin	Btub-F	AACCTCCATTCAGGAGATGTTT	[43]
	Btub-R	TCTGCTGTAGCATCCTGGTATT	

antibacterial effect of synthesised components, rGO–Cu and rGO–Zn, was evaluated to evaluate the synergic effect of Cu and Zn. The bacterial suspension was mixed with materials rGO–Cu, rGO–Zn and rGO–Cu–Zn at the final concentrations of 1.00%, 0.50% and 0.25% and incubated as described above. Bacterial growth was judged by the naked eye.

For the in-planta experiment, the tomato plants cv. Mandat F1 was used at the stage of four true leaves and nanocomposite rGO–Cu–Zn. The plants were grown in the substrate TS4 (Klasmann–Deilmann GmbH, Geeste, Germany) at 26 °C (16-h days) and 22 °C (8-h nights). The plants were sprayed with 1.00% nanomaterial dispersion until dripping off and then left to dry overnight. Champion 50 WG was applied at a concentration of 7 g L^{-1} dispersion according to the manufacturer's recommendation. A suspension of *X. euvesicatoria* 2594 ($1 \cdot 10^8$ CFU mL^{-1} in PBS) was sprayed on the plants analogously to the nanomaterial application. The plants were covered by transparent plastic bags for 48 h to increase humidity. For the positive control, the nanomaterial was replaced by sterile water. For each treatment, 12 plants were tested, and the experiment was performed in three repetitions. The evaluation of BS symptoms was carried out two weeks after plant inoculation. The occurrence of the symptoms was determined using a 4-point scale. Based on the obtained data, the disease severity (*DS*) was calculated using the following formula:

$$DS(\%) = \frac{\sum \left(number\ of\ plants\ in\ a\ disease\ scale\ point \cdot disease\ scale\ point \right)}{\left(total\ number\ of\ plants \cdot maximum\ disease\ scale\ point \right)} \cdot 100$$

BS symptoms evaluation: 0 = healthy leaves without symptoms, 1 = low symptoms occurrence (1–3 spots per leaf), 2 = symptoms occupying up to 1/3 of leaf area, 3 = high incidence of symptoms (more than one third of the leaf surface infected).

Effect of rGO–Cu–Zn on relative gene expression in tomato plants

The effect of rGO–Cu–Zn was evaluated based on the expression of five different plant genes using real-time PCR. As an individual treatment for evaluating phytotoxicity and gene expression, represented plants were sprayed with 10% rGO–Cu–Zn; other plant treatments were prepared analogously as described in the antibacterial activity. RNA extraction was performed immediately after the first appearance of black spot symptoms. Symptomatic plant parts, namely leaves and parts of stems, were taken and immediately deposited at − 80 °C. Plant tissue was homogenised in a mortar with a pestle using liquid nitrogen. In total, 100 mg of homogenised plant tissue from each sample was utilised for RNA extraction using the Spectrum Plant Total RNA Kit (Sigma–Aldrich, St. Louis, MO, USA) according to the manufacturer's protocol. Reverse transcription was performed using 200 ng of RNA, random hexamer primers (Roche, Basel, Switzerland) and RevertAid Reverse Transcriptase (Thermo Fisher Scientific, Waltham, MA, USA), according to the manufacturer. The cDNA was used as a template for the real-time PCR, with the primer pairs shown in Table 1. Housekeeping gene beta tubulin was used to normalise gene expression among the samples. The real-time PCR reaction of a 20 µl volume consisted of 1 × HotSybr qPCR Kit (MCLab, San Francisco, CA, USA), 2 µl of

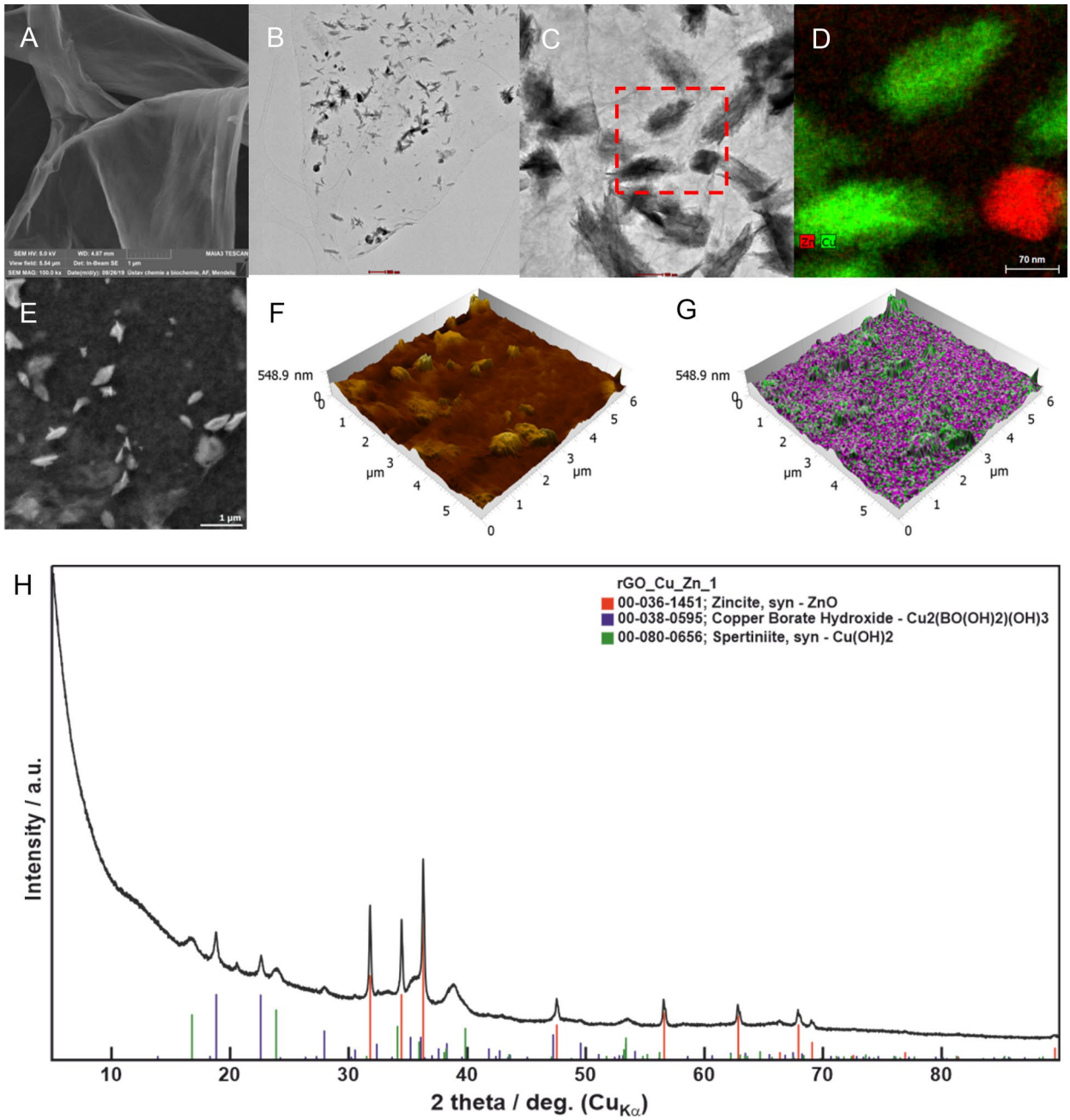

Fig. 1 SEM image of GO **A**, TEM images of rGO-Cu–Zn **B** and **C** and elemental mapping of rGO-Cu–Zn **D** of the marked area cut from the TEM image —The correlative analysis SEM **E**, AFM **F** and EDS **G** of rGO-Cu–Zn – XRPD of rGO-Cu–Zn (H)

prepared cDNA, 0.3 µm of each primer of the primer pair and PCR grade water. The reactions for each sample were prepared in duplicate and run in qTower real-time PCR cycler (Analytik Jena, Jena, Germany). The cycling conditions were 10 min at 95 °C, 40 cycles of 15 s at 95 °C and 1 min at 60 °C. The Livak and Schmittgen [38] method was used for relative quantification, and the analyses were performed using qPCRsoft 3.4 software (Analytik Jena, Jena, Germany).

Results and discussion

This study's plant protection material consisted of several components. As mentioned, copper could not be omitted for its effects, but it could be used in orders

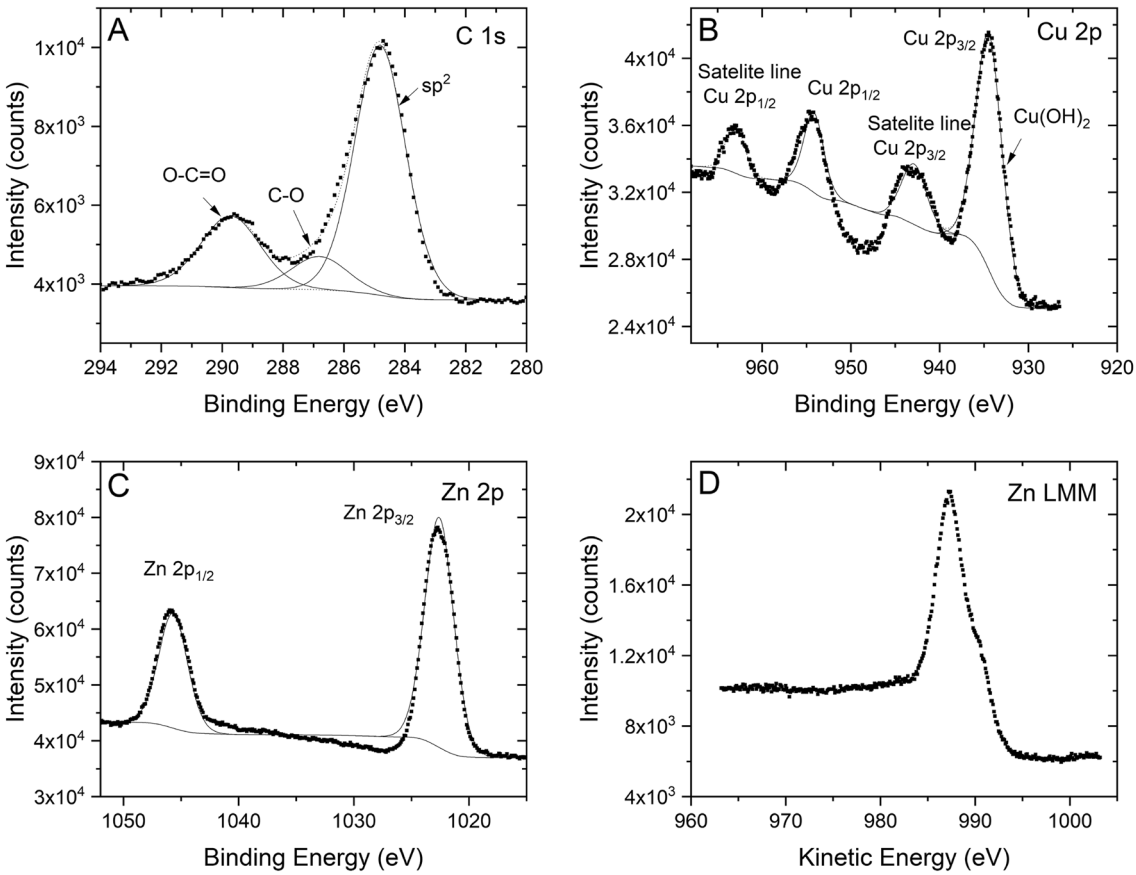

Fig. 2 XPS spectra of C 1 s **A**, Cu 2p **B**, Zn 2p and Zn LMM **D** regions of nanocomposite rGO-Cu–Zn

Table 2 The concentration of copper, zinc, and boron in nanocomposites quantified using ICP-MS

Sample	Concentration (mg/L)		
	Cu	Zn	B
rGO–Cu–Zn	1430	1455	77
rGO–Cu	2560	–	65
rGO–Zn	–	2903	127

Table 3 Bacterial growth of *X. euvesicatoria* 2594 in the presence of nanocomposite and commercial preparation,

Treatment	Cu content (mg L^{-1})	Concentration (%)	Bacterial growth (%)
rGO–Cu–Zn	10.07	1.50	0.00
	6.71	1.00*	0.23
	3.36	0.50	19.78
	1.68	0.25	61.78
Champion 50 WG	50	0.01*	0.00
	25	0.005	16.65
	12.5	0.0025	62.01
Control	–	–	100.00

* MIC that killed 99% of bacteria

of magnitude, smaller amounts accompanied by controlled release. Copper was used as NPs because they are more effective at lower concentrations than in bulk due to their favourable volume-to-surface ratio. Another part of the material represented zinc NPs. Like copper, zinc is a naturally occurring element in plants and animals. Some microorganisms are more sensitive to zinc and, thus, are more effective than copper in some cases [44]. If zinc accompanies copper, they can synergise when both elements are effective in noticeably smaller amounts than if applied separately. The last but essential part of the study's material was rGO, which carried oxygen functional groups on its surface. Copper and zinc NPs were bonded onto GO using these functional groups with a simultaneous reduction of GO, which resulted in rGO. The synthesis of rGO–Cu–Zn preceded the synthesis of GO by modified Tour's method. The GO (Fig. 1A) exhibited a typical smooth surface and large-size sheets. The synthesis of nanocomposite included the one-step

decoration of GO with two different metal-based NPs. Copper and Zinc NPs were bonded onto GO from their precursors, which were reduced by sodium borohydride while simultaneously reducing GO to form the rGO–Cu–Zn nanocomposite. The sheet of rGO decorated with NPs is shown in the TEM image in Fig. 1B, and the detailed morphology of NPs on rGO is shown in Fig. 2C. Elemental mapping of the cutout from the TEM image with detailed NPs (Fig. 1D) confirmed the presence of both types of NPs. The nanocomposites with only one type of metal NPs were also synthesised to verify the synergistic effect of the combination of Copper NPs and Zinc NPs. The SEM images confirm the successful synthesis of rGO–Cu (Additional file 1: Fig. S1A) and rGO–Zn (Additional file 1: Fig. S1B). AFM topography studies were carried out together with SEM and EDX elemental

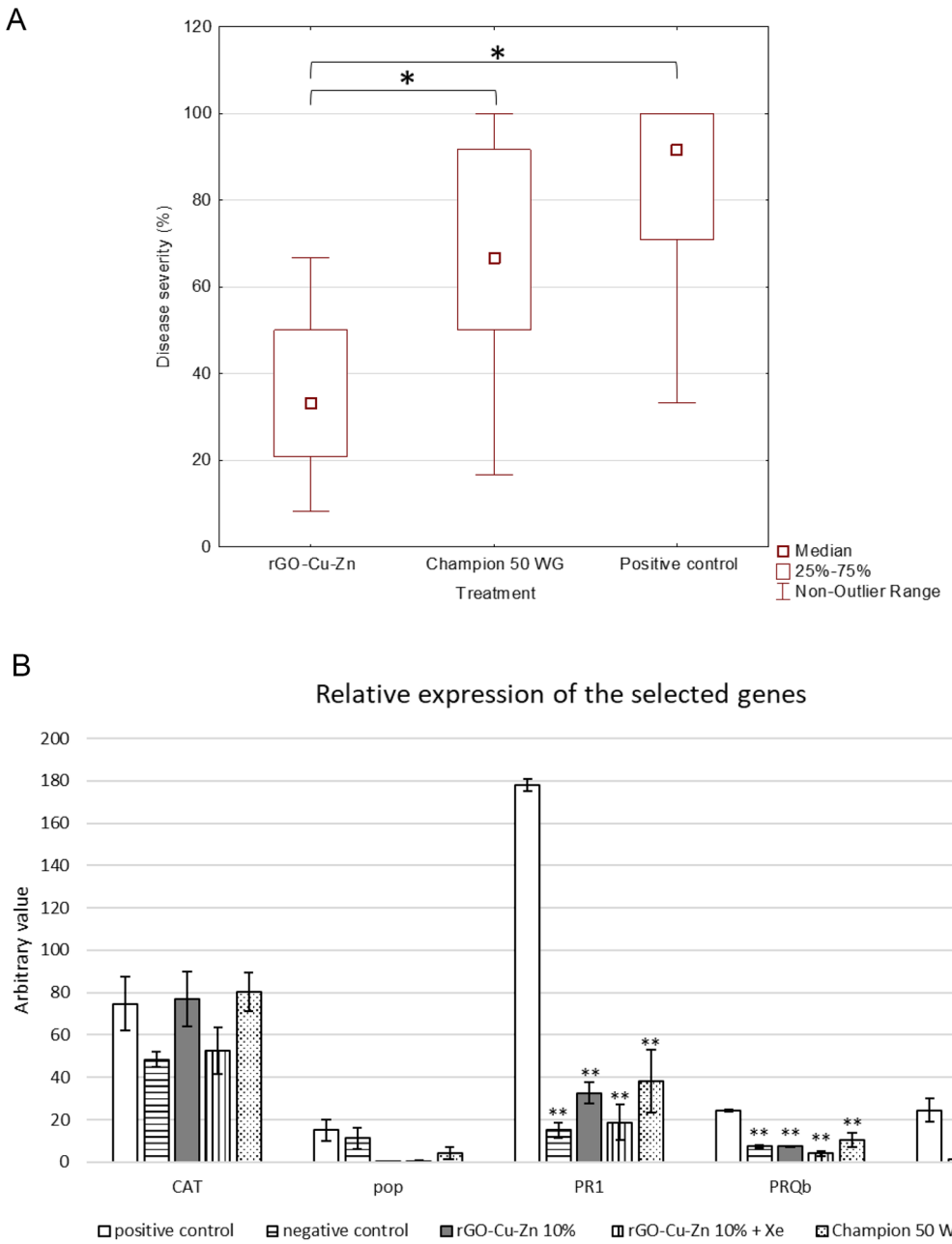

Fig. 3 Summarisation of the DS in the in-planta experiment **A**—Gene expression of tomato after the application of nanocomposite and commercial preparation (single-factor ANOVA, $p < 0.05$; Tukey's test, $p < 0.05$) **B** —— ** represents the statistical difference ($p < 0.01$) compared with positive control of the respective analysed gene

analysis. Figure 1E shows the topography of the nanocomposite. AFM-combined SEM (Fig. 1F) correlates with EDX (Fig. 1G), where the fuchsia colour represents the presence of zinc, and the green colour represents the presence of copper. The SEM image for correlative microscopy is in Fig. 1E. The AFM study revealed a random distribution of powder particles ranging from 1 µm up to 2 µm in size. Ultra-fine particles of Copper and Zinc were randomly distributed. The XRD powder diffraction in Fig. 1H reveals the successful reduction of GO because a characteristic GO peak is missing [45]. Zinc NPs were in the expected ZnO form, and Copper NPs were found in two forms. The first form of Copper NPs was $Cu(OH)_2$, and the second form was $Cu_2[BO(OH)_2](OH)_3$ (PDF-4+,# 00–038-0595), which had been probably created due to the presence of sodium borohydride as a reducing agent. $Cu_2[BO(OH)_2](OH)_3$ is also known as a mineral Jacquesdietrichit. The boron residues probably came from the reducing agent sodium borohydride, and the boron was probably incorporated into the structure of nanocomposites. The boron residues that could not be removed using intensive washing with ultrapure water were also present in all tested nanocomposites (rGO–Cu and rGO–Zn) (Table 2). The results from ICP-MS also show the ratio between copper and zinc in rGO–Cu–Zn was almost 1:1.

The results from the XPS analysis confirmed the XRD analysis results. Characteristic XPS spectra of the major components (C 1 s, Cu 2p, Zn 2 p and Zn LMM Auger peak) are presented in Fig. 2. The high-resolution spectrum reveals three peaks in the C 1 s region (Fig. 2A): a sp^2 peak at 284.81 eV, a peak at 286.81 eV attributed to C–O and a high binding energy peak at 289.73 eV, indicating C=O group [46, 47]. As shown in Fig. 2B, the binding energies of Cu $2p_{3/2}$ (934.41 eV) and Cu $2p_{1/2}$ (954.16 eV) with two strong satellites (942.88 eV and 963.00 eV) and a difference of 19.75 eV could be attributed to the chemical state of Cu^{2+} in $Cu(OH)_2$ [48]. Figure 2C shows the XPS spectra of the Zn 2p region. The Zn 2p XPS spectrum exhibits the Zn $2p_{3/2}$ region at 1022.59 eV and the Zn $2p_{1/2}$ region at 1045.70 eV with a 23.10 eV difference. As the asymmetry of the Zn $2p_{3/2}$ peak shape may vary, the analysis of Zn LMM Auger peaks is commonly employed to identify the chemical states of zinc species. Auger peaks tend to exhibit more pronounced changes in shape compared with XPS peaks due to the involvement of three electrons and many body effects in a single Auger transition. Figure 2D presents the characteristic Auger Zn spectrum of ZnO NPs, centred at a kinetic energy of 987.78 eV [49].

Antibacterial properties of the nanocomposite

Bacterial growth in percentage represents the CFU number in treated variants in comparison to a positive control (Table 3). Concentrations of rGO–Cu–Zn (0.25–1.5%) and Champion 50 WG (0.0025–0.01%) showed strong antibacterial activity. The results in Table 3 display the relation between bacterial growth and the corresponding copper content of both preparations. MIC for the rGO–Cu–Zn was determined at the concentration of 1%, which corresponds to 6.71 mg Cu L^{-1}. MIC for the Champion 50 WG was defined at the concentration of 0.01% (50 mg Cu L^{-1}).

Important factors for their use in plant disease management must be considered to develop novel antibacterial nanomaterials. The effective antibacterial concentration of nanomaterial should be lower than other preparations. In the in-vitro experiment, the nanocomposite exhibited an equivalent antibacterial activity when compared with Champion 50 WG, but with a several times lower amount of Cu. The evaluation of the rGO–Cu and rGO–Zn components confirmed the synergistic effect of the Cu and Zn contained in the rGO–Cu–Zn nanocomposite. Total bacterial growth inhibition was observed for the rGO–Cu–Zn (1% (w/v) dispersion), whereas the components at the same concentration inhibited but did not eradicate all the bacteria colonies (Additional file 1: Fig. S2).

The other factor assuming the functionality of antibacterial preparation should include fast eradication of the pathogen cells from the host tissue, preventing the development of plant disease symptoms. Figure 3A summarizes the results of in-planta experiments and the occurrence of the BS symptoms. A decrease in the DS was observed in both types of treatment. The median DS for the untreated control was more than 91%. In the case of commercial preparation, the median DS was more than 66%. Application of the rGO–Cu–Zn significantly decreased the occurrence of the BS symptoms, where the DS median value was almost 34%.

Many studies deal with the antibacterial properties of NPs in which *Bacillus* sp., *E.coli* or *Staphylococcus* sp. are probably the most often used genera [50, 51]. The genus *Xanthomonas* is also an often-used model bacteria, but the antibacterial activity of the composite nanomaterials containing copper and zinc is presented to a lesser extent. Alswat et al. showed the antibacterial effect of zeolite nanocomposite containing a copper oxide and ZnO concentration of 10 mg mL^{-1} [52]. Jiao et al. presented the antimicrobial activity of copper/zinc-loaded montmorillonite at a concentration > 300 mg L^{-1} [53]. Ashfaq et al. used 1 mg ml^{-1} of carbon nanofibers decorated by copper

and zinc NPs completely to inhibit bacterial growth [54]. Carvalho et al. published high antibacterial activity of Cu/Zn hybrid NPs (100–500 ug mL^{-1}) against BS caused by *X. perforans* on tomato plants. In the latter study, the authors presented a reduction of BS disease severity up to 80%. In this study's in-planta experiment, the plants treated with nanocomposite showed more than a 62% reduction of DS compared with the control [55].

The negative effects are the other important factors that should be considered. The application of the novel preparations should not trigger the symptoms of phytotoxicity in the plants. Several studies refer to the benefits and negatives of nanomaterials in plants [56–59]. Symptoms of phytotoxicity were reported after applying the Cu-based nanocomposites [16]. White spots or crinkled leaves appeared on peppers treated by core–shell Cu and fixed-quat Cu composites at concentrations > 100 µg mL^{-1}. On the contrary, the mixed-valence Cu composite and Kocide 3000 used in the same study did not cause phytotoxicity, even at 500 µg $mL^{-}1$ concentration. The results of [16] are analogous to this study's in-planta experiment where no phytotoxicity was noticed even after the application of rGO–Cu–Zn at a 10 times higher dose than MIC (67,1 mg Cu·L^{-1}), neither for the Champion 50 WG. To evaluate the negative effect of the rGO–Cu–Zn on the molecular level, the expression of the genes associated with the action of abiotic and biotic stress factors was analyzed. Gene expression in the plants treated with 10% nanocomposite did not exhibit a noticeable increase. The genes *CAT* and *PR1* were slightly more expressed than the negative control. Based on the results in Fig. 3B, certain similarities in the gene expression profile between the negative control and treated plants should be considered. Except for the *CAT*, a significant increase in gene expression was observed in the case of positive control.

The manifestation of the application of rGO–Cu–Zn was very pronounced at polyphenol oxidase (*POP*) and *PR1*, which encodes the glucan endo-1, 3-beta-D-glucosidase. The expression of *PR1* was almost 15 times higher, and *POP* was even 50 times higher in the positive control compared with the plants treated by rGO–Cu–Zn and inoculated by bacteria. Expression of *PRQb*, the sequence encoding the gene for the formation of the basic form of beta-1, 3-glucanase class III, is more than eight times higher. For the *TomQ* gene expressing the acid form of beta-1, 3-glucanase class III, the expression was evaluated as more than 16 times higher. The results of gene expression are analogous to those of the previous study [60], where no phytotoxicity was noticed after the application of rGO–Cu–Ag nanocomposite but [61] presented phytotoxicity of GO–silver nanocomposite at the concentration of 200 µg mL^{-1}.

The interaction of plant cells with the nanomaterials results in the modification of gene expression, which can negatively involve plant metabolism, growth and development. Changes in plant biochemical pathways depend on the ability of the NPs to penetrate inside the plant, which is probably one of the major factors for the interaction with the cell structures [62, 63]. Moreover, the effect of phytotoxicity can vary depending on the plant species [64]. No phytotoxicity symptoms of the tomato plants and no negative effect on the gene level were observed in the study. The structure of the nanocomposite can explain this. Copper and Zinc NPs are probably not released from the GO matrix, keeping the effectiveness of the nanocomposite tethered directly on the plant surface. The hypothesis corresponds to [16], where the mixed valence Cu composites did not demonstrate phytotoxicity. Moreover, the accumulation of the GO in mesophyll and parenchyma cells of the leaf or stem was disproved [65]. This also complies with [66], where no phytotoxicity of graphene nanocomposite GO–Fe_3O_4 was observed even at 1000 µg ml^{-1} concentration. Furthermore, the positive effects on the plant growth and development of GO are pointed out in [67–69] or [70].

Conclusion

This newly synthesized plant protective rGO–Cu–Zn nanocomposite consists of several components, and each of them plays a significant role in the protection and complements one another appropriately while all components are naturally occurring. Currently, copper cannot be omitted entirely for its effects on agriculture, but it is possible to apply it in several times smaller amounts and use it more smartly. An advantage of utilizing the nanocomposite is that it results in a DS of infected plants nearly three times lower than the control group and almost twice lower than when using the commercial product Champion 50 WG. This study's results indicate a reduction in the *X. euvesicatoria* inoculum in tomato plants, which is consistent with the significant antibacterial effect of the nanocomposite. Moreover, the effective amount of copper in rGO–Cu–Zn was approximately 6.7 mg Cu L^{-1}. In comparison, the commercial product was less effective at approx. 3500 mg Cu L^{-1}. Furthermore, the treated tomato plants observed no phytotoxicity or negative effects of rGO–Cu–Zn on the gene expression. Therefore, composite materials based on nano-carbon can be promising in plant protection. In this study, the ability of the synthesised rGO–Cu–Zn nanocomposite to suppress *X. euvesicatoria* has been showcased. However, it is also essential to evaluate this nanocomposite's effectiveness on a broader range of bacterial and fungal plant pathogens.

Supplementary Information

The online version contains supplementary material available at https://doi.org/10.1186/s40538-023-00489-2.

Additional file 1: Fig S1. Scanning electron microscopy images of reduced graphene oxide (rGO-Cu) (A), and reduced graphene oxide with zinc nanoparticles (rGO-Zn) (B). **Fig S2.** The evaluation of the antibacterial effect of the rGO-Cu and rGO-Zn components.

Acknowledgements
This work was supported by the European Regional Development Fund Multidisciplinary research to increase application potential of nanomaterials in agricultural practice (No. CZ.02.1.01/0.0/0.0/16_025/0007314) and by the Ministry of Education, Youth and Sports of the Czech Republic. The authors acknowledge the assistance the Research Infrastructure NanoEnviCz provided, supported by the Ministry of Education, Youth and Sports of the Czech Republic under project No. LM2018124 and CzechNanoLab Research Infrastructure supported by project No. LM2023051. The authors would like to acknowledge Pavel Švec for scanning electron microphotographs and Radka Pechancová from Palacký University Olomouc, who performed the ICP-MS analysis. The authors would like to acknowledge Pavel Komarov (NenoVision s.r.o.) for carrying out the AFM-in-SEM multimodal correlative analysis (CPEM) by LiteScope™.

Author contributions
ZB: conceptualization, Methodology, Writing—Original Draft, Investigation; JP: methodology, Writing—Original Draft, Investigation; DT: formal analysis, Data Curation; JP: visualization, Data Curation; AR: formal analysis, Data Curation; PB: visualization, Formal analysis,TK: formal analysis, Data Curation; AE: writing—Review & Editing; VA: supervision, Writing—Review & Editing; LR: supervision, Writing—Review & Editing.

Funding
European Regional Development Fund No. CZ.02.1.01/0.0/0.0/16_025/000731 4. Ministry of Education, Youth and Sports of the Czech Republic LM2018124. Ministry of Education, Youth and Sports of the Czech Republic No. LM2023051.

Availability of data and materials
The datasets used and/or analyzed during the current study are available from the corresponding author on reasonable request.

Declarations

Ethics approval and consent to participate
Not applicable.

Consent for publication
Not applicable.

Competing interests
The authors declare that they have no competing interests.

Author details
[1]Department of Chemistry and Biochemistry, Mendel University in Brno, Zemědělská 1, 613 00 Brno, Czech Republic. [2]Central European Institute of Technology, Brno University of Technology, Purkyňova 123, 612 00 Brno, Czech Republic. [3]Department of Microelectronics, Faculty of Electrical Engineering and Communication, Brno University of Technology, Technická 3058/10, 616 00 Brno, Czech Republic. [4]Institute of Inorganic Chemistry of the Czech Academy of Sciences, Husinec-Řez 1001, 250 68 Husinec-Řez, Czech Republic. [5]Mendeleum – Institute of Genetics, Faculty of Horticulture, Mendel University in Brno, Valtická 334, 69144 Lednice, Czech Republic. [6]Department of Fruit Science, Mendel University in Brno, Valtická 334, 691 44 Lednice, Czech Republic.

Received: 25 July 2023 Accepted: 8 October 2023
Published online: 24 October 2023

References

1. Wu X, Yu L, Pehrsson PR. Are processed tomato products as nutritious as fresh tomatoes? Scoping review on the effects of industrial processing on nutrients and bioactive compounds in tomatoes. Adv Nutr. 2022;13(1):138–51.
2. FAO. 2020. https://www.fao.org/faostat/en/#data.
3. Blomme G, et al. Bacterial diseases of bananas and enset: current state of knowledge and integrated approaches toward sustainable management. Front Plant Sci. 2017. https://doi.org/10.3389/fpls.2017.01290.
4. Matsumoto H, et al. Bacterial seed endophyte shapes disease resistance in rice. Nature Plants. 2021;7(1):60–72.
5. Sundin GW, et al. Bacterial disease management: Challenges, experience, innovation and future prospects. Mol Plant Pathol. 2016;17(9):1506–18.
6. Moretti C, Amatulli MT, Buonaurio R. PCR-based assay for the detection of Xanthomonas euvesicatoria causing pepper and tomato bacterial spot. Lett Appl Microbiol. 2009;49(4):466–71.
7. Osdaghi E, et al. Occurrence and characterization of the bacterial spot pathogen Xanthomonas euvesicatoria on pepper in Iran. J Phytopathol. 2016;164(10):722–34.
8. Potnis N, et al. Bacterial spot of tomato and pepper: diverse Xanthomonas species with a wide variety of virulence factors posing a worldwide challenge. Mol Plant Pathol. 2015;16(9):907–20.
9. Balogh B, et al. Improved efficacy of newly formulated bacteriophages for management of bacterial spot on tomato. Plant Dis. 2003;87(8):949–54.
10. Jones JB, et al. Reclassification of the Xanthomonads associated with bacterial spot disease of tomato and pepper. Syst Appl Microbiol. 2004;27(6):755–62.
11. Osdaghi E, et al. A centenary for bacterial spot of tomato and pepper. Mol Plant Pathol. 2021;22(12):1500–19.
12. Horvath DM, et al. Transgenic resistance confers effective field level control of bacterial spot disease in tomato. PLoS ONE. 2012;7(8): e42036.
13. Jones J, et al. Survival of Xanthomonas campestris pv. vesicatoria in Florida on tomato crop residue, weeds, seeds, and volunteer tomato plants. Phytopathology. 1986;76(4):430–4.
14. Pohronezny K, Volin RB. The effect of bacterial spot on yield and quality of fresh market tomatoes1. HortScience. 1983;18(1):69–70.
15. Silveira PR, et al. Physiological changes in tomato leaves arising from Xanthomonas gardneri infection. Physiol Mol Plant Pathol. 2015;92:130–8.
16. Fan Q, et al. Antibacterial effect of copper composites against Xanthomonas euvesicatoria. Crop Prot. 2021;139: 105366.
17. Ritchie DF. Bacterial spot of pepper and tomato. The Plant Health Instructor. 2000. https://doi.org/10.1094/PHI-I-2000-1027-01.
18. Grass G, Rensing C, Solioz M. Metallic copper as an antimicrobial surface. Appl Environ Microbiol. 2011;77(5):1541–7.
19. European Commission, Commission implementing regulation (EU) 2018/1981 2018.
20. Lamichhane JR, et al. Thirteen decades of antimicrobial copper compounds applied in agriculture. A review Agronomy for Sustainable Development. 2018. https://doi.org/10.1007/s13593-018-0503-9.
21. Gayon U, Sauvageau C. Notice sur la vie et les travaux de A. Millardet [Note on the life and work of A. Millardet]. Memoires de la Societe des Sciences Physiques et Naturelles de Bordeaux. 1903;6:9–47.
22. Mackie KA, Muller T, Kandeler E. Remediation of copper in vineyards—a mini review. Environ Pollut. 2012;167:16–26.
23. Richardson HW. Handbook of copper compounds and applications. Boca Raton: CRC Press; 1997.
24. Arman P, Wain RL. Studies upon the copper fungicides X. The role of leaf exudates in the solution of copper from Bordeaux mixture. Ann Appl Biol. 1958;46(3):366–74.
25. Bae E, et al. Bacterial cytotoxicity of the silver nanoparticle related to physicochemical metrics and agglomeration properties. Environ Toxicol Chem. 2010;29(10):2154–60.
26. Khot LR, et al. Applications of nanomaterials in agricultural production and crop protection: a review. Crop Prot. 2012;35:64–70.
27. Siddiqui Z, et al. Effects of zinc oxide nanoparticles (ZnO NPs) and some plant pathogens on the growth and nodulation of lentil (Lens culinaris Medik.). Acta Phytopathologica et Entomol Hungarica. 2018;53(2):195–211.

28. Siddiqui ZA, et al. Titanium dioxide and zinc oxide nanoparticles affect some bacterial diseases, and growth and physiological changes of beetroot. Int J Veg Sci. 2019;25(5):409–30.
29. Cakmak I, McLaughlin MJ, White PJ. Zinc for better crop production and human health. Plant Soil. 2017;411(1–2):1–4.
30. Maywald M, Rink L. Zinc in human health and infectious diseases. Biomolecules. 2022. https://doi.org/10.3390/biom12121748.
31. Younas N, et al. Alleviation of zinc deficiency in plants and humans through an effective technique; biofortification: a detailed review. Acta Ecol Sin. 2022. https://doi.org/10.1016/j.chnaes.2022.07.008.
32. Hu W, et al. Remediation of zinc-contaminated soils by using the two-step washing with citric acid and water-soluble chitosan. Chemosphere. 2021. https://doi.org/10.1016/j.chemosphere.2021.131092.
33. Bytesnikova Z, et al. Reduced graphene oxide-based nanometal-composite containing copper and silver nanoparticles protect tomato and pepper against Xanthomonas euvesicatoria infection. Chem Biol Technol Agric. 2022. https://doi.org/10.1186/s40538-022-00347-7.
34. Hammerschmiedt T, et al. Impact of smart combinations of graphene oxide and micro/nanosized sulfur particles on soil health and plant biomass accumulation. Chem Biol Technol Agric. 2022. https://doi.org/10.1186/s40538-022-00323-1.
35. Tougaard S. Practical guide to the use of backgrounds in quantitative XPS. J Vacuum Sci Technol A. 2021. https://doi.org/10.1116/6.0000661.
36. Degen T, et al. The HighScore suite. Powder Diffr. 2014;29:S13–8.
37. ICDD, PDF-4+ 2023 International Centre for Diffraction Data. Newtown Square. USA: PA; 2022.
38. Livak KJ, Schmittgen TD. Analysis of relative gene expression data using real-time quantitative PCR and the 2(-Delta Delta C(T)) method. Methods. 2001;25(4):402–8.
39. Ishihara T, et al. Transcriptome analysis of quantitative resistance-specific response upon Ralstonia solanacearum infection in tomato. PLoS ONE. 2012;7(10): e46763.
40. Uehara T, et al. Resistant and susceptible responses in tomato to cyst nematode are differentially regulated by salicylic acid. Plant Cell Physiol. 2010;51(9):1524–36.
41. Parker J, et al. Quantitative proteomics of tomato defense against Pseudomonas syringae infection. Proteomics. 2013;13(12–13):1934–46.
42. Rademacher W. Plant growth regulators: backgrounds and uses in plant production. J Plant Growth Regul. 2015;34(4):845–72.
43. Løvdal T, Lillo C. Reference gene selection for quantitative real-time PCR normalization in tomato subjected to nitrogen, cold, and light stress. Anal Biochem. 2009;387(2):238–42.
44. McDevitt CA, et al. A molecular mechanism for bacterial susceptibility to zinc. PLoS Pathog. 2011. https://doi.org/10.1371/journal.ppat.1002357.
45. Yasin G, et al. Exploring the nickel–graphene nanocomposite coatings for superior corrosion resistance: manipulating the effect of deposition current density on its morphology, mechanical properties, and erosion-corrosion performance. Adv Eng Mat. 2018. https://doi.org/10.1002/adem.201701166.
46. Bytešníková Z, et al. New insight into the biocompatibility/toxicity of graphene oxides and their reduced forms on *Chlamydomonas reinhardtii*. NanoImpact. 2023. https://doi.org/10.1016/j.impact.2023.100468.
47. Mukherjee S, et al. Silver nanoparticle-decorated reduced graphene oxide nanomaterials exert membrane stress and induce immune response to inhibit the early phase of hiv-1 infection. Adv Mat Interfaces. 2023. https://doi.org/10.1002/admi.202201996.
48. Kang JH, et al. Tubular Cu(OH)2 arrays decorated with nanothorny Co–Ni bimetallic carbonate hydroxide supported on Cu foam: a 3D hierarchical core-shell efficient electrocatalyst for the oxygen evolution reaction. J Mat Chem A. 2018;6(21):10064–73.
49. Sahai A, Goswami N. Probing the dominance of interstitial oxygen defects in ZnO nanoparticles through structural and optical characterizations. Ceram Int. 2014;40(9):14569–78.
50. Hajipour MJ, et al. Antibacterial properties of nanoparticles. Trends Biotechnol. 2012;30(10):499–511.
51. Mba IE, Nweze EI. Nanoparticles as therapeutic options for treating multidrug-resistant bacteria: Research progress, challenges, and prospects. World J Microbiol Biotechnol. 2021;37(6):108.
52. Alswat AA, Ahmad MB, Saleh TA. Preparation and characterization of zeolite\zinc oxide-copper oxide nanocomposite: antibacterial activities. Colloid Interface Sci Commun. 2017;16:19–24.
53. Jiao L, et al. Preparation, characterization, antimicrobial and cytotoxicity studies of copper/zinc-loaded montmorillonite. J Animal Sci Biotechnol. 2017;8(1):27.
54. Ashfaq M, Verma N, Khan S. Copper/zinc bimetal nanoparticles-dispersed carbon nanofibers: a novel potential antibiotic material. Mater Sci Eng C. 2016;59:938–47.
55. Carvalho R, et al. Bactericidal activity of copper-zinc hybrid nanoparticles on copper-tolerant Xanthomonas perforans. Sci Rep. 2019;9(1):20124.
56. Vochita G, et al. Graphene oxide effects in early ontogenetic stages of *Triticum aestivum L*. seedlings. Ecotoxicol Environ Safety. 2019;181:345–52.
57. Chen J, et al. Various physiological response to graphene oxide and amine-functionalized graphene oxide in wheat (*Triticum aestivum*). Molecules. 2018. https://doi.org/10.3390/molecules23051104.
58. Guo X, et al. Effects of graphene oxide on tomato growth in different stages. Plant Physiol Biochem. 2021;162:447–55.
59. You Y, et al. Graphene oxide decreases Cd concentration in rice seedlings but intensifies growth restriction. J Hazard Mater. 2021;417: 125958.
60. Bytešníková Z, et al. Reduced graphene oxide-based nanometal-composite containing copper and silver nanoparticles protect tomato and pepper against Xanthomonas euvesicatoria infection. Chem Biol Technol Agric. 2022;9(1):84.
61. Strayer A, et al. Low concentrations of a silver-based nanocomposite to manage bacterial spot of tomato in the greenhouse. Plant Dis. 2015;100(7):1460–5.
62. Yu J, et al. Current trends and challenges in the synthesis and applications of chitosan-based nanocomposites for plants: a review. Carbohyd Polym. 2021;261: 117904.
63. Nair R, et al. Nanoparticulate material delivery to plants. Plant Sci. 2010;179(3):154–63.
64. Young M, Santra S. Copper (Cu)–silica nanocomposite containing valence-engineered Cu: A new strategy for improving the antimicrobial efficacy of Cu biocides. J Agric Food Chem. 2014;62(26):6043–52.
65. Zhao S, et al. Toxicity and translocation of graphene oxide in Arabidopsis thaliana. Environ Toxicol Pharmacol. 2015;39(1):145–56.
66. Wang X, et al. Graphene oxide-Fe3O4 nanocomposites as high-performance antifungal agents against *Plasmopara viticola*. Sci China Mater. 2017;60(3):258–68.
67. Park S, et al. Graphene oxide-assisted promotion of plant growth and stability. Nanomaterials. 2020. https://doi.org/10.3390/nano10040758.
68. Li J, et al. The mutual effects of graphene oxide nanosheets and cadmium on the growth, cadmium uptake and accumulation in rice. Plant Physiol Biochem. 2020;147:289–94.
69. Mahmoud NE, Abdelhameed RM. Superiority of modified graphene oxide for enhancing the growth, yield, and antioxidant potential of pearl millet (*Pennisetum glaucum L*) under salt stress. Plant Stress. 2021;2:100025.
70. Gao M, et al. Foliar graphene oxide treatment increases photosynthetic capacity and reduces oxidative stress in cadmium-stressed lettuce. Plant Physiol Biochem. 2020;154:287–94.

Publisher's Note